LU TP 99–16
hep-ph/9907299
July 1999

Jet Production by Virtual Photons[1]

C. Friberg

Department of Theoretical Physics, Lund University,
Helgonavägen 5, S-223 62 Lund, Sweden
christer@thep.lu.se

Abstract

The production of jets is studied in collisions of virtual photons, γ^*p and $\gamma^*\gamma^*$, specifically for applications at HERA and LEP2. Photon flux factors are convoluted with matrix elements involving either direct or resolved photons and, for the latter, with parton distributions of the photon. Special emphasis is put on the range of uncertainty in the modeling of the resolved component. The resulting model is compared with existing data.

[1]To appear in the Proceedings of the International Conference on the Structure and Interactions of the Photon; Photon 99, 23-27 May 1999, Freiburg im Breisgau, Germany.

1 Introduction

The photon is a complicated object to describe. In the DIS region, i.e. when it is very virtual, it can be considered as devoid of any internal structure, at least to first approximation. In the other extreme, the total cross section for real photons is dominated by the resolved component of the wave function, where the photon has fluctuated into a $\mathrm{q\overline{q}}$ state. The nature of this resolved component is still not well understood, especially not the way in which it dies out with increasing photon virtuality. This dampening is likely not to be a simple function of virtuality, but to depend on the physics observable being studied, i.e. on the combination of subprocesses singled out.

Since our current understanding of QCD does not allow complete predictability, one sensible approach is to base ourselves on QCD-motivated models, where a plausible range of uncertainty can be explored. Hopefully comparisons with data may then help constrain the correct behaviour. The ultimate goal therefore clearly is to have a testable model for all aspects of the physics of $\gamma^*\mathrm{p}$ and $\gamma^*\gamma^*$ collisions. As a stepping stone towards constructing such a framework, in this paper we explore the physics associated with the production of 'high-$p_\perp$' jets in the collision. That is, we here avoid the processes that only produce activity along the $\gamma^*\mathrm{p}$ or $\gamma^*\gamma^*$ collision axis. For resolved photons this corresponds to the 'soft' or 'low-$p_\perp$' events of the hadronic physics analogy, for direct ones to the lowest-order DIS process $\gamma^*\mathrm{q} \to \mathrm{q}$.

The processes that we will study here instead can be exemplified by $\gamma^*\gamma^* \to \mathrm{q\overline{q}}$ (direct), $\gamma^*\mathrm{g} \to \mathrm{q\overline{q}}$ (single-resolved for $\gamma^*\gamma^*$, direct for $\gamma^*\mathrm{p}$) and $\mathrm{gg} \to \mathrm{q\overline{q}}$ (double-resolved for $\gamma^*\gamma^*$, (single-)resolved for $\gamma^*\mathrm{p}$), where the gluons come from the parton content of a resolved virtual photon or from the proton. Note that these are multi-scale processes, at least involving the virtuality Q_i^2 of either photon ($i = 1, 2$) and the $p_\perp^2$ of the hard subprocess. For a resolved photon, the relative transverse momentum $k_\perp$ of the initial $\gamma^* \to \mathrm{q\overline{q}}$ branching provides a further scale, at least in our framework.

Almost real photons allow long-lived $\gamma^* \to \mathrm{q\overline{q}}$ fluctuations, that then take on the properties of non-perturbative hadronic states, specifically of vector mesons such as the ρ^0. It is therefore that an effective description in terms of parton distributions becomes necessary. Hence the resolved component of the photon, as opposed to the direct one. That such a subdivision is more than a technical construct is excellently illustrated by the x_γ^{obs} plots from HERA [1].

The resolved photon can be further subdivided into low-virtuality fluctuations, which then are of a nonperturbative character and can be represented by a set of vector mesons, and high-virtuality ones that are describable by perturbative $\gamma^* \to \mathrm{q\overline{q}}$ branchings. The former is called the VMD (vector meson dominance) component and the latter the anomalous one. The parton distributions of the VMD component are unknown from first principles, and thus have to be based on reasonable ansätze, while the anomalous ones are perturbatively predictable.

The traditional tool for handling such complex issues is the Monte Carlo approach. Our starting point is the model for real photons [2] and the parton distribution parameterizations of real and virtual photons [3] already present in the PYTHIA [4] generator. Several further additions and modifications have been made to model virtual photons, as will be described in the following [5].

2 The Model

The cross sections for the processes ep $\to$ e**X** and ee $\to$ ee**X** can be written as the convolutions [6, 7, 8]

$$\mathrm{d}\sigma(\mathrm{ep} \to \mathrm{e}\mathbf{X}) = \sum_{\xi=\mathrm{T,L}} \iint \mathrm{d}y\,\mathrm{d}Q^2\; f^{\xi}_{\gamma/\mathrm{e}}(y,Q^2)\;\mathrm{d}\sigma(\gamma^*_{\xi}\mathrm{p} \to \mathbf{X}) \tag{1}$$

and

$$\mathrm{d}\sigma(\mathrm{ee} \to \mathrm{ee}\mathbf{X}) = \sum_{\xi_1,\xi_2=\mathrm{T,L}} \iiiint \mathrm{d}y_1\mathrm{d}Q_1^2\mathrm{d}y_2\,\mathrm{d}Q_2^2\; f^{\xi_1}_{\gamma/\mathrm{e}}(y_1,Q_1^2) f^{\xi_2}_{\gamma/\mathrm{e}}(y_2,Q_2^2)\mathrm{d}\sigma(\gamma^*_{\xi_1}\gamma^*_{\xi_2} \to \mathbf{X}). \tag{2}$$

The flux of photons $f(y,Q^2)$ (see y definition below) from the lepton is factorized from the subprocess cross sections involving the virtual photon, $\gamma^*\mathrm{p} \to \mathbf{X}$ and $\gamma^*\gamma^* \to \mathbf{X}$. The sum is over the transverse and longitudinal photon polarizations. For ep events, this factorized ansatz is perfectly general, so long as azimuthal distributions in the final state are not studied in detail. In $\mathrm{e^+e^-}$ events, it is not a good approximation when the virtualities Q_1^2 and Q_2^2 of both photons become of the order of the squared invariant mass W^2 of the colliding photons [9].

When Q^2/W^2 is small, one can derive [10, 8, 9]

$$f^{\mathrm{T}}_{\gamma/l}(y,Q^2) = \frac{\alpha_{\mathrm{em}}}{2\pi}\left(\frac{(1+(1-y)^2}{y}\frac{1}{Q^2} - \frac{2m_l^2 y}{Q^4}\right)\;, \tag{3}$$

$$f^{\mathrm{L}}_{\gamma/l}(y,Q^2) = \frac{\alpha_{\mathrm{em}}}{2\pi}\frac{2(1-y)}{y}\frac{1}{Q^2}\;. \tag{4}$$

The y variable is defined as the lightcone fraction the photon takes of the incoming lepton momentum. The lepton scattering angle θ_i is related to Q_i^2, where the kinematical limits on Q_i^2 are, unless experimental conditions reduce the θ range, $Q^2_{i,\mathrm{min}} \approx \frac{y^2}{1-y}m_{\mathrm{e}}^2$ and $Q^2_{i,\mathrm{max}} \approx (1-y)s$.

Within the allowed region, the phase space is Monte Carlo sampled according to $(\mathrm{d}Q^2/Q^2)\,(\mathrm{d}y/y)\,\mathrm{d}\varphi$, with the remaining flux factor combined with the cross section factors to give the event weight used for eventual acceptance or rejection.

The hard-scattering processes are classified according to whether one or both photons are resolved. For the direct process $\gamma^*_{\xi_i}\gamma^*_{\xi_i} \to \mathrm{f\bar{f}}$, f some fermion, the cross sections for transverse and longitudinal photons are used [11, 5]. Remember that the cross section for a longitudinal photon vanishes as Q_i^2 in the limit $Q_i^2 \to 0$.

For a resolved photon, the photon virtuality scale is included in the arguments of the parton distribution but, in the spirit of the parton model, the virtuality of the parton inside the photon is not included in the matrix elements. Neither is the possibility of the partons being in longitudinally polarized photons (see below, however). The same subprocess cross sections can therefore be used for direct $\gamma^*\mathrm{p}$ processes and for single-resolved $\gamma^*\gamma^*$ ones. Both transverse and longitudinal photons are considered for the QCD Compton $\gamma^*\mathrm{q} \to \mathrm{gq}$ and boson–gluon fusion $\gamma^*\mathrm{g} \to \mathrm{q\bar{q}}$ processes [12, 5]. The matrix elements are then convoluted with parton distributions.

Finally we come to resolved processes in $\gamma^*\mathrm{p}$ and doubly-resolved ones in $\gamma^*\gamma^*$. There are six basic QCD cross sections, $\mathrm{qq'} \to \mathrm{qq'}$, $\mathrm{q\bar{q}} \to \mathrm{q'\bar{q}'}$, $\mathrm{q\bar{q}} \to \mathrm{gg}$, $\mathrm{qg} \to \mathrm{qg}$, $\mathrm{gg} \to \mathrm{gg}$ and $\mathrm{gg} \to \mathrm{q\bar{q}}$. The same subprocess cross sections as those known from pp physics [13] can therefore be used. Again, a convolution with parton distributions is necessary.

One major element of model dependence enters via the choice of parton distributions for a resolved virtual photon. These distributions contain a hadronic component that is not perturbatively calculable. It is therefore necessary to parameterize the solution with input from experimental data, which mainly is available for (almost) real photons. In the following we will use the SaS distributions [3], which are the ones best suited for our formalism. Another set of distributions is provided by GRS [14], while a simpler recipe for suppression factors relative to real photons has been proposed by DG [15].

The SaS distributions for a real photon can be written as

$$f_a^{\gamma}(x,\mu^2) = \sum_V \frac{4\pi\alpha_{\rm em}}{f_V^2} f_a^{\gamma,V}(x,\mu^2;Q_0^2) + \frac{\alpha_{\rm em}}{2\pi} \sum_{\rm q} 2e_{\rm q}^2 \int_{Q_0^2}^{\mu^2} \frac{{\rm d}k^2}{k^2}\, f_a^{\gamma,{\rm q}\overline{\rm q}}(x,\mu^2;k^2) \ . \quad (5)$$

Here the sum is over a set of vector mesons $V = \rho^0, \omega, \phi, {\rm J}/\psi$ according to a vector-meson-dominance ansatz for low-virtuality fluctuations of the photon, with experimentally determined couplings $4\pi\alpha_{\rm em}/f_V^2$. The higher-virtuality, perturbative, fluctuations are represented by an integral over the virtuality k^2 and a sum over quark species. We will refer to the first part as the VMD one and the second as the anomalous one.

From the above ansatz, the extension to a virtual photon is given by the introduction of a dipole dampening factor for each component,

$$\begin{aligned} f_a^{\gamma^*}(x,\mu^2,Q^2) &= \sum_V \frac{4\pi\alpha_{\rm em}}{f_V^2} \left(\frac{m_V^2}{m_V^2+Q^2}\right)^2 f_a^{\gamma,V}(x,\mu^2;\tilde{Q}_0^2) \\ &+ \frac{\alpha_{\rm em}}{2\pi} \sum_{\rm q} 2e_{\rm q}^2 \int_{Q_0^2}^{\mu^2} \frac{{\rm d}k^2}{k^2} \left(\frac{k^2}{k^2+Q^2}\right)^2 f_a^{\gamma,{\rm q}\overline{\rm q}}(x,\mu^2;k^2) \ . \end{aligned} \quad (6)$$

Thus, with increasing Q^2, the VMD components die away faster than the anomalous ones, and within the latter the low-k^2 ones faster than the high-k^2 ones.

Since the probed real photon is purely transverse, the above ansatz does not address the issue of parton distributions of the longitudinal virtual photons. One could imagine an ansatz based on longitudinally polarized vector mesons, and branchings $\gamma_{\rm L}^* \to {\rm q}\overline{\rm q}$, but currently no parameterization exists along these lines. We will therefore content ourselves by exploring alternatives based on applying a simple multiplicative factor R to the results obtained for a resolved transverse photon. As usual, processes involving longitudinal photons should vanish in the limit $Q^2 \to 0$. To study two extremes, the region with a linear rise in Q^2 is defined either by $Q^2 < \mu^2$ or by $Q^2 < m_\rho^2$, where the former represents the perturbative and the latter some non–perturbative scale. Also the high-Q^2 limit is not well constrained; we will compare two different alternatives, one with an asymptotic fall-off like $1/Q^2$ and another which approaches a constant ratio, both with respect to the transverse resolved photon. (Since we put $f_a^{\gamma^*}(x,\mu^2,Q^2) = 0$ for $Q^2 > \mu^2$, the R value will actually not be used for large Q^2, so the choice is not so crucial.) We therefore study the alternative ansätze

$$R_1(y,Q^2,\mu^2) = 1 + a\frac{4\mu^2Q^2}{(\mu^2+Q^2)^2}\frac{f_{\gamma/l}^{\rm L}(y,Q^2)}{f_{\gamma/l}^{\rm T}(y,Q^2)} \ , \quad (7)$$

$$R_2(y,Q^2,\mu^2) = 1 + a\frac{4Q^2}{(\mu^2+Q^2)}\frac{f_{\gamma/l}^{\rm L}(y,Q^2)}{f_{\gamma/l}^{\rm T}(y,Q^2)} \ , \quad (8)$$

$$R_3(y,Q^2,\mu^2) = 1 + a\frac{4Q^2}{(m_\rho^2+Q^2)}\frac{f_{\gamma/l}^{\rm L}(y,Q^2)}{f_{\gamma/l}^{\rm T}(y,Q^2)} \quad (9)$$

with $a = 1$ as main contrast to the default $a = 0$. The y dependence compensates for the difference in photon flux between transverse and longitudinal photons.

Another ambiguity is the choice of μ^2 scale in parton distributions. Based on various considerations, we compare three different alternatives:

$$\mu_1^2 = p_\perp^2 \frac{\hat{s} + Q_1^2 + Q_2^2}{\hat{s}} \ , \qquad \mu_2^2 = p_\perp^2 + Q_1^2 + Q_2^2 \ , \qquad \mu_3^2 = 2\mu_1^2 \ . \tag{10}$$

Only the second alternative ensures $f_a^{\gamma^*}(x, \mu^2, Q^2) > 0$ for arbitrarily large Q^2; in all other alternatives the resolved contribution (at fixed $p_\perp$) vanish above some Q^2 scale. The last alternative exploits the well-known freedom of including some multiplicative factor in any (leading-order) scale choice. When nothing is mentioned explicitly below, the choice μ_1^2 is used.

The issues discussed above are the main ones that distinguish the description of processes involving virtual photons from those induced by real photons or by hadrons in general. In common is the need to consider the buildup of more complicated partonic configurations from the lowest-order 'skeletons' defined above, (*i*) by parton showers, (*ii*) by multiple parton–parton interactions and beam remnants, where applicable, and (*iii*) by the subsequent transformation of these partons into the observable hadrons. The latter, hadronization stage can be described by the standard string fragmentation framework [16], followed by the decays of unstable primary hadrons, and is not further discussed here. The parton shower, multiple-interaction and beam-remnant aspects are discussed elsewhere [5].

3 Comparisons with Data

In this section the model is compared with data. We will not make a detailed analysis of experimental results but use it to point out model dependences and to constrain some model parameters.

3.1 Inclusive Jet Cross Sections

Inclusive ep jet cross sections have been measured by the H1 collaboration [17] in the kinematical range $0 < Q^2 < 49$ GeV^2 and $0.3 < y < 0.6$. For $\mathrm{d}\sigma_{\mathrm{ep}}/\mathrm{d}E_\perp^*$ data is available in nine different Q^2 bins; two of them are shown here, Fig. 1, with similar results for the intermediate bins. The plots were produced with the HzTool [18] package. The $E_\perp^*$ and η^* are calculated in the γ^*p centre of mass frame where the incident proton direction corresponds to positive η^*. The SaS 1D parton distribution together with a few different μ_i scales are used to model the resolved photon component.

In the highest Q^2 bin the direct component gives the dominant contribution. However, the resolved component is not negligible. All the scales μ_i depend on the photon virtuality. This gives a larger resolved component in this region as compared to the conventional choice, $\mu = p_\perp$. In the low Q^2 bin the μ_1 and μ_2 scales do not differ much from $p_\perp$ and the cross sections are in nice agreement with data. The cross section with the μ_3 scale overshoots the data in this region.

Changing the photon parton distribution from SaS 1D to SaS 2D will give a slightly lower result for the low-Q^2 bins. A comparison has been made with the GRS LO [14] parton distribution [5] and, in its region of validity, differences are small. One could imagine larger differences for γ^* parton distributions that from the onset are more different.

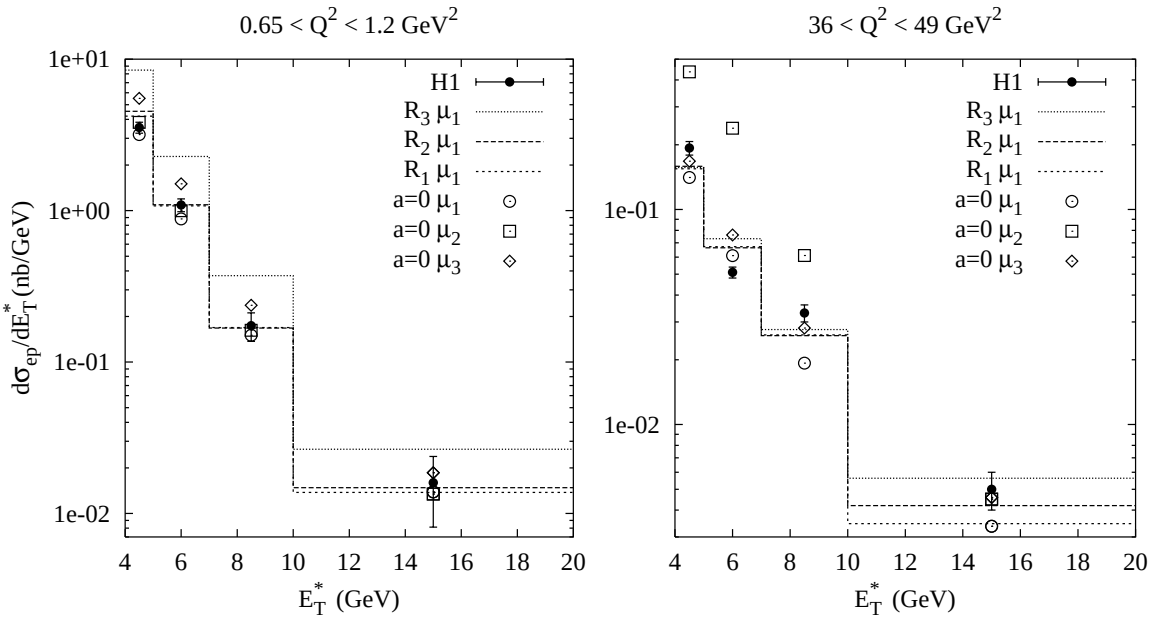

Figure 1: The differential jet cross section $\mathrm{d}\sigma_{\mathrm{ep}}/\mathrm{d}E^*_\perp$ for jets with $-2.5 < \eta^* < -0.5$ and $0.3 < y < 0.6$. $a = 0$ indicates that only transversely polarized resolved photons are considered.

Using a parton distribution for a real photon cannot describe the Q^2 dampening in the distributions shown in this section.

Using CTEQ 3L instead of GRV 94 LO (which is default in PYTHIA) as the proton parton distribution reduces the result in some $E^*_\perp$ bins by half. The GRV 94 HO parton distribution give a slightly lower result (as compared to GRV 94 LO). The differences mainly come from the gluon distributions, that are not yet so well constrained from data. In the modeling of the parton distributions, it is a deceptive accident that the more well-known proton parton distribution gives a larger uncertainty than the photon one. It offers a simple example that also phenomenology of other areas may directly influence the interpretation of photon data.

The OPAL collaboration has measured inclusive one–jet and two–jet cross sections in the range $|\eta^{\mathrm{jet}}| < 1$ and requiring $E^{\mathrm{jet}}_\perp$ to be larger than 3 GeV [19]. The centre of mass energies were 130 and 136 GeV. The inclusive jet cross sections as a function of $E^{\mathrm{jet}}_\perp$ or η^{jet} are compared with data [5], with events generated at $\sqrt{s_{\mathrm{ee}}} = 133$ GeV.

At low $E^{\mathrm{jet}}_\perp$ the double–resolved events are dominating and at larger $E^{\mathrm{jet}}_\perp$ it is the direct processes since more energy goes into the hard scattering in the latter case. For single–resolved events, the SaS 1D VMD component dies out much quicker with increasing $E^{\mathrm{jet}}_\perp$ than the SaS 2D one which is comparable with the direct–anomalous events at high $E^{\mathrm{jet}}_\perp$. For both cases, at high $E^{\mathrm{jet}}_\perp$, the direct–anomalous components give the same order of magnitude contribution to the cross section as the double–resolved events. The biggest difference between the two parton distributions can be seen at low $E^{\mathrm{jet}}_\perp$ and for the $|\eta^{\mathrm{jet}}|$ distributions, where the double–resolved events dominate; it is a reflection of the difference in normalization among the contributions. For the SaS 2D case, this kinematical region makes the VMD component more important than the anomalous one; as a consequence multiple interactions play an important role. The double–resolved contribution for SaS 2D

without multiple interaction is reduced by half. Clearly, for the SaS 1D case the opposite is true: the importance of the components are reversed. In the region of high $E_\perp^{\rm jet}$, where the direct events dominate, the model is undershooting data. On the other hand, there is nice agreement with data for the $|\eta^{\rm jet}|$ distribution when using SaS 2D.

3.2 Forward Jet Cross Sections

Jet cross sections as a function of Bjorken-x, $x_{\rm Bj}$, for forward jet production (in the proton direction) have been measured at HERA [20]. The objective is to probe the dynamics of the QCD cascade at small $x_{\rm Bj}$. The forward jet is restricted in polar angle w.r.t. the proton and the transverse momenta $p_\perp^{\rm jet}$ should be of the same order as the virtuality of the photon, suppressing an evolution in transverse momenta. If the jet has a large energy fraction of the proton there will be a big difference in x between the jet and the photon vertex; $x_{\rm Bj} \ll x_{\rm jet}$, allowing an evolution in x. The above restrictions will not eliminate the possibility of having a resolved photon, although the large Q^2 values are not in favour of it.

The HzTool routines were used to obtain the results in Fig. 2. A larger forward jet cross section is obtained with a stronger Q^2 dependence for the hard scale, with $\mu_2^2 = p_\perp^2 + Q^2$ in best agreement with data [21]. The choice of scale does not only affect the resolved photon contribution but also the direct photon, arising from the scale dependence in the proton parton distribution. The rather large Q^2 values, $Q^2 \simeq (p_\perp^{\rm jet})^2$, suppresses VMD photons and favours the SaS 1D distribution which is the one used here, though the difference is small.

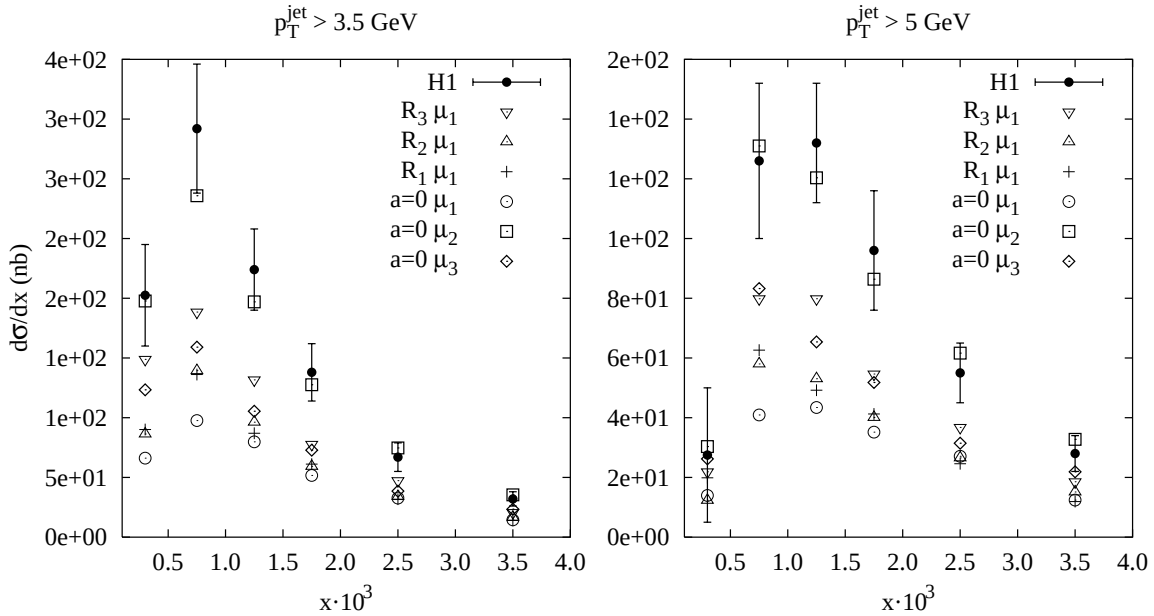

Figure 2: Forward jet cross section as a function of x. The results with three different alternatives of longitudinal resolved photons R_i are compared with purely transverse ones, $a = 0$, and data from H1.

Note that the μ_3 scale undershoots the forward jet cross section data and overshoots the inclusive jet distributions at low Q^2, so it is not a real alternative. As a further

check, with more data accumulated and analysed, the $(p_\perp^{\rm jet})^2/Q^2$ interval could be split into several subranges which hopefully would help to discriminate between scale choices.

With the experience of forward jets at HERA, we suggest a similar study at LEP. The optimal kinematical and forward jet constraints have to be set by each collaboration itself; we will only estimate the order of magnitude for the cross section and point out uncertainties in the model.

Comparing with forward jets at HERA, one of the leptons will play the role of the proton. Some of the constraints can be taken over directly, for example, $x_{\rm jet} = E_{\rm jet}/E_{\rm e} > 0.035$ and $0.5 < (p_\perp^{\rm jet})^2/Q^2 < 2$. To fulfill the jet selection one of the leptons has to be tagged in order to know the virtuality of the photon. To obtain a reasonable number of events the other lepton is not tagged. With a centre of mass energy of 200 GeV, the smallest accessible $x_{\rm Bj} = \frac{Q^2}{ys}$ is around 10^{-4}, where Q^2 and y is calculated from the tagged electron, omitting the virtuality of the other photon. In a more sophisticated treatment also double–tagged events are analyzed; then one of the photons plays the role of a proton and the forward jet should be defined with respect to one of the photons.

As for the case at HERA, the μ_2 scale gives the largest forward jet cross section, about twice as large as with the μ_1 scale [5]. Most of the differences arise from the double–resolved events. Double–resolved and single–resolved events, where the resolved photon give rise to the forward jet, dominate the forward jet cross section. At low x, for the μ_2 scale, the double–resolved contribution is close to an order of magnitude larger than the direct one. For the μ_1 scale it is about a factor of four. As for the case at HERA, the rise of the forward jet cross section at small x is dominated by resolved photons. A study like this at LEP could be an important cross check for the understanding of resolved photons and that of small-x dynamics.

3.3 Importance of longitudinal resolved photons

In this section we will study the importance of longitudinal resolved photons. A sensible Q^2–dependent scale choice, μ_1, together with the SaS 1D distribution will be used throughout.

With $a = 1$ the different alternatives are shown in Fig. 1 for the $\mathrm{d}\sigma_{\rm ep}/\mathrm{d}E_\perp^*$ distributions together with the result from pure transverse photons, i.e. $a = 0$. The importance of the resolved contributions decreases with increasing Q^2 which makes the asymptotic behaviour less crucial. The onset of longitudinal photons governed by the R_1 and R_2 alternatives are favoured whereas the R_3 one overshoots data in the context of the other model choices made here.

In Fig. 2 the same alternatives are shown for the forward jet cross sections. With this scale choice, μ_1, none of the longitudinal resolved components (together with the direct contribution) are sufficient to describe the forward jet cross section. The resolved contribution with R_3 is about the same as the one obtained with the scale $\mu_2^2 = p_\perp^2 + Q^2$ (without longitudinal contribution); the difference in the total results originates from the difference in the direct contributions. With R_1 and $a = 1$, the μ_2 scale (not shown) overshoots the data. The above study indicates, as expected, that longitudinal resolved photons are important for detailed descriptions of various distributions. It cannot by itself explain the forward jet cross section, but may give a significant contribution. Combined with other effects, for example, different scale choice, parton distributions and underlying events, it could give a reasonable description. The model(s) so far does not take into account the difference in x distribution or the k^2 scale (of the $\gamma^* \to \mathrm{q\overline{q}}$ fluctuations) be-

tween transverse and longitudinal photons. As long as the distributions under study allow a large interval in x the average description may be reasonable. In a more sophisticated treatment these aspects have to be considered in more detail.

4 Summary and Outlook

The plan here is to have a complete description of the main physics aspects in γp and $\gamma\gamma$ collisions, which will allow important cross checks to test universality of certain model assumptions. As a step forward, we have here concentrated on those that are of importance for the production of jets by virtual photons, and are absent in the real-photon case. While we believe in the basic machinery developed and presented here, we have to acknowledge the many unknowns — scale choices, parton distribution sets (also those of the proton), longitudinal contributions, underlying events, etc. — that all give non-negligible effects. To make a simultaneous detailed tuning of all these aspects was not the aim here, but rather to point out model dependences that arise from a virtual photon.

When Q^2 is not small, naively only the direct component needs to be treated, but in practice a rather large contribution arises from resolved photons. For example, for high-Q^2 studies like forward jet cross sections, Fig. 2, or inclusive differential jet cross sections, Fig. 1. Resolved longitudinal photons are poorly understood and the model presented here can be used to estimate their importance and get a reasonable global description. Longitudinal effects are in most cases small but of importance for fine–tuning.

The inclusive $\gamma^*\gamma^*$ one-jet and two-jet cross sections are well described except for the high $E_\perp^{\rm jet}$ region of the $E_\perp^{\rm jet}$ distribution [5]. In this region, the direct events are dominating. Currently, owing to the lesser flexibility in the modeling of the direct component, we do not see any simple way to improve the model. The factorized ansatz made for the photon flux is expected to be valid in this kinematical range; interference terms are suppressed by $Q_1^2Q_2^2/W^2_{\gamma^*\gamma^*}$. However, differences in the application of the cone jet algorithm may affect the results.

The forward jet cross section presented by H1 [20] is well described by an ordinary parton shower prescription including the possibility of having resolved photons. The criteria that the $p_\perp^{\rm jet}$ should be of the same order as Q^2, makes the scale choice crucial and $\mu_2^2 = p_\perp^2 + Q^2$ is favoured by data, as concluded in [21]. With this experience we predict the forward jet cross section to be obtained at LEP [5]. With more data accumulated and analyzed, the $(p_\perp^{\rm jet})^2/Q^2$ interval could be split into several subranges, which hopefully would help to discriminate between different scale choices.

Multiple interactions for the anomalous component are not yet included, and is not expected to be of same importance as in the VMD case. However, for low k^2 fluctuations it may be important, especially for SaS 1D, and need to be investigated.

After this study of jet production by virtual photons it is natural to connect it together with low–$p_\perp$ events. Clearly, a smooth transition from perturbative to non–perturbative physics is required. Further studies are needed and will be presented in a future publication.

Acknowledgements

We acknowledge helpful conversations with, among others, Jon Butterworth, Jiri Chýla, Gerhard Schuler, Hannes Jung, Leif Jönsson, Ralph Engel and Tancredi Carli.

References

[1] ZEUS Collaboration, M. Derrick et al., Phys. Lett. **B322** (1994) 287;
H1 Collaboration, T. Ahmed et al., Nucl. Phys. **B445** (1995) 195.

[2] G.A. Schuler and T. Sjöstrand,
Nucl. Phys. **B407** (1993) 539; Z. Phys. **C73** (1997) 677.

[3] G.A. Schuler and T. Sjöstrand,
Z. Phys. **C68** (1995) 607; Phys. Lett. **B376** (1996) 193.

[4] T. Sjöstrand, Computer Phys. Commun. **82** (1994) 74;
http://www.thep.lu.se/∼torbjorn/Pythia.html.

[5] C. Friberg and T. Sjöstrand, LU TP 99–11 (hep-ph/9907245), submitted to Eur. Phys. J. **C**.

[6] C.F. von Weiszäcker, Z. Phys. **88** (1934) 612.

[7] E.J. Williams, Phys. Rev. **45** (1934) 729.

[8] V.M. Budnev, I.F. Ginzburg, G.V. Meledin and V.G. Serbo, Phys. Rep. **15** (1975) 181.

[9] G.A. Schuler, Computer Phys. Commun. **108** (1998) 279.

[10] G. Bonneau, M. Gourdin and F. Martin, Nucl. Phys. **B54** (1973) 573.

[11] V.N. Baier, E.A. Kuraev, V.S. Fadin and V.A. Khoze, Phys. Rep. **78** (1981) 293.

[12] G. Altarelli and G. Martinelli, Phys. Lett. **76B** (1978) 89;
A. Mendéz, Nucl. Phys. **B145** (1978) 199;
R. Peccei and R. Rückl, Nucl. Phys. **B162** (1980) 125;
Ch. Rumpf, G. Kramer and J. Willrodt, Z. Phys. **C7** (1981) 337.

[13] B.L. Combridge, J. Kripfganz and J. Ranft, Phys. Lett. **70B** (1977) 234;
R. Cutler and D. Sivers, Phys. Rev. **D17** (1978) 196.

[14] M. Glück, E. Reya and M. Stratmann, Phys. Rev. **D51** (1995) 3220.

[15] F.M. Borzumati and G.A. Schuler, Z. Phys. **C58** (1993) 139;
M. Drees and R.M. Godbole, Phys. Rev. **D50** (1994) 3124.

[16] B. Andersson, G. Gustafson, G. Ingelman and T. Sjöstrand, Phys. Rep. **97** (1983) 31.

[17] H1 Collaboration, C. Adloff et al., Phys. Lett. **B415** (1997) 418.

[18] J. Bromley et al., HzTool — A Package for Monte Carlo Generator – Data Comparison at HERA,
http://dice2.desy.de/∼h01rtc/hztool.html

[19] OPAL Collaboration, K. Ackerstaff et al., Z. Phys. **C73** (1997) 433.

[20] H1 Collaboration, C. Adloff et al., Nucl. Phys. **B538** (1998) 3;
H1 Collaboration, S. Aid et al., Phys. Lett. **B356** (1995) 118;
ZEUS Collaboration, J. Breitweg et al., Eur. Phys. J. **C6** (1998) 239.

[21] H. Jung, L. Jönsson and H. Kuster, DESY 98-051 (hep-ph/9805396); DESY 99-028 (hep-ph/9903306), to appear in Eur. Phys. J. **C**.